Acta Cryst. (1997). A53, 202–216

Analysis of Diffuse Scattering *via* the Reverse Monte Carlo Technique: a Systematic Investigation

TH. PROFFEN AND T. R. WELBERRY

Research School of Chemistry, Australian National University, Canberra, ACT 0200, Australia. E-mail: proffen@rsc.anu.edu.au

(Received 31 July 1996; accepted 6 November 1996)

Abstract

The viability of using the reverse Monte Carlo (RMC) method for quantitative analysis of the diffuse X-ray or neutron scattering from single crystals of disordered materials is investigated. The method has been applied to a number of two- and three-dimensional model examples in which both occupational and displacement disorder are present separately and in combination. While occupational or displacement disorder are each separately handled well, with the RMC simulation reproducing the input correlation structure of the models quite effectively, more difficulty was encountered when the different types of disorder were present in combination. In this case, it was necessary to employ a strategy where the occupation shifts and displacement shifts were carried out alternately with no more than 10% of the crystal being visited before switching between the two modes. It was also found to be advantageous to exclude all high-angle diffraction data when assessing occupation shifts. Furthermore, a new method of modelling distortions by swapping the displacements of two atom sites rather than shifting each atom individually was found to produce chemically more realistic bond-length distributions.

1. Introduction

The analysis of Bragg diffraction data reveals only information about the *average* crystal structure, such as atomic positions, temperature factors and site occupancies. Diffuse scattering contains additional information about static or thermal disorder within the crystal. However, the interpretation of diffuse scattering is in general difficult. An overview of the different methods used to analyse diffuse scattering can be found in the review papers by Welberry & Butler (1994, 1995).

One approach that has been used extensively in this laboratory employs Monte Carlo (MC) simulation (Metropolis, Rosenbluth, Rosenbluth, Teller & Teller, 1953) to model the disordered structure under investigation (see Welberry & Butler, 1994). In this method, a real-space computer model, based on realistic physical and chemical criteria, is set up in terms of parameters describing the basic interatomic or intermolecular interactions. Realizations of the model are obtained *via* computer simulation. The diffraction pattern of the model structure is computed and compared with the observed pattern. The model is iteratively adjusted until a 'match' is obtained. The method has been used with success to obtain a greater understanding of a diverse range of materials (Welberry & Butler, 1994, 1995). The main advantages of this technique over other treatments of diffuse scattering are that, first of all, it allows systematic exploration of different possible causes of any observed diffuse scattering but, most importantly, allows a more physical picture of the disordered structure to be obtained. One drawback, however, is that, although in principle it should be possible to perform the iterative adjustment of the model automatically, this task is still beyond the computational resources currently available.

A quite different approach to the analysis of diffuse scattering data has emerged in recent years, the so-called reverse Monte Carlo (RMC) method, developed by McGreevy & Pusztai (1988). In this method, the difference between observed and calculated diffuse scattering intensities is minimized as a function of the positions and occupancies of the atomic sites in the model crystal, rather than the total energy of the crystal as is the case in direct MC. The method has been applied to a variety of systems but until recently the analysis of diffuse scattering using RMC was mainly confined to powder diffraction data (Nield, Keen, Hayes & McGreevy, 1992, 1993; Montfrooij, McGreevy, Hadfield & Anderson, 1996). The application of RMC to diffuse *single-crystal* scattering data was first reported in a neutron diffraction study by Nield, Keen & McGreevy (1995). This study shows that RMC is potentially a powerful tool for the analysis of diffuse scattering from single crystals. It appears that, though requiring substantial computer resources, the method is viable using present-day computers. The present work was therefore undertaken to assess the efficacy of the RMC method when applied to the sort of systems we are interested in which show chemical disorder and subsequent relaxations.

One of the systems that has figured prominently in our research in recent years is that of cubic stabilized zirconias (CSZ's), and our initial intention was to apply the RMC method to this system. Cubic stabilized zirconia (Welberry, Withers, Thompson & Butler, 1992; Welberry, Butler, Thompson & Withers, 1993; Welberry, Withers & Mayo, 1995; Neder, Frey & Schulz, 1990;

ISSN 0108-7673

Proffen, Neder, Frey & Assmus, 1993; Proffen, Neder & Frey, 1996) exhibits complex diffuse scattering patterns resulting from oxygen–vacancy ordering followed by relaxations of the neighbouring atoms. A program for RMC simulations has been developed (Proffen & Neder, 1997) that allows occupational disorder and positional relaxations to be modelled simultaneously for this kind of system. Some preliminary RMC simulations of diffuse neutron scattering of calcium-stabilized zirconia ($Zr_{0.85}Ca_{0.15}O_{1.85}$) resulted in a good agreement between observed and calculated intensity after refining the oxygen–vacancy and Zr–Ca ordering and the subsequent displacements, but the resulting structure turned out to be very unlikely from a chemical point of view. Those calculations are far from finished, but at this stage it seemed important to undertake a more systematic study of the capabilities and/or limitations of the RMC technique for different kinds of disorder. It was also apparent that for a systematic study the fully three-dimensional (3D) CSZ system required more computing than could be utilized in a reasonable time frame. Consequently, it was decided to carry out tests on some model systems that were constructed to contain different types and combinations of disorder analogous to, but rather simpler than, those in CSZ's. In this paper, we present the results of RMC calculations carried out on these two-dimensional and three-dimensional 'test' structures, and discuss the implications for extending the work to real CSZ systems.

2. Monte Carlo (MC) and reverse Monte Carlo (RMC) simulations

In this section, we give a brief outline of the two simulation methods. While the paper is mainly concerned with RMC, the comparison with direct MC is an important aspect of our work, but in addition the 'test' examples used were generated *via* MC.

2.1. *Monte Carlo (MC)*

The total energy of the crystal is expressed as a function of random variables such as site occupancies or displacements from the average structure. The algorithm is based on the original Metropolis Monte Carlo technique (Metropolis *et al.*, 1953). A site within the crystal is chosen at random and the associated variables are altered by some random amount. The energy difference ΔE of the configuration before and after the change is computed. The new configuration is accepted if the transition probability P given by (1) is greater than a random number η, chosen uniformly in the range [0, 1].

$$P = \exp(-\Delta E/kT)/[1 + \exp(-\Delta E/kT)]. \quad (1)$$

In (1), T is the temperature and k Boltzmann's constant. It should be noted that the value of the temperature T controls the proportion of accepted modifications that lead to a larger total energy. The process is repeated until the system reaches its equilibrium. In this paper, we refer to a single MC (or RMC) step as 'move', whereas the number of moves necessary to visit every crystal site once on average will be called one 'cycle'.

2.2. *Reverse Monte Carlo (RMC)*

The scattered intensity is first calculated from the chosen crystal starting configuration and a goodness-of-fit parameter χ^2 is computed:

$$\chi^2 = \sum_{i=1}^{N} [I_e(\mathbf{Q}_i) - I_c(\mathbf{Q}_i)]^2/\sigma^2. \quad (2)$$

The sum is over all measured data points $\mathbf{Q}_i$, I_e stands for the experimental and I_c for the calculated intensity. As for the MC method, the RMC simulation proceeds with the selection of a random site within the crystal. The system variables associated with this site, such as occupancy or displacement, are changed by a random amount, and then the scattering intensity and the goodness-of-fit parameter χ^2 are recalculated. The change $\Delta\chi^2$ of the goodness of fit χ^2 before and after the generated move is computed. Every move that improves the fit ($\Delta\chi^2 < 0$) is accepted. 'Bad' moves worsening the agreement between observed and calculated intensities are accepted with a probability $P = \exp(-\Delta\chi^2/2)$. The parameter σ has an effect similar to the temperature T in MC simulations and controls the proportion of 'bad' moves to be accepted. The RMC process is repeated until χ^2 converges to its minimum.

2.3. *Computational aspects*

The RMC algorithm presented by Nield *et al.* (1995) formed the basis for the development of the RMC software used in this paper. In order to achieve the maximum degree of flexibility, the RMC routines were integrated in the defect structure simulation program *DISCUS* (Proffen & Neder, 1997). For practical use, it is necessary to include a scaling factor f and a background parameter b in the previous definition of the goodness of fit χ^2 [(2)]. If a weighting scheme is also applied, the expression for χ^2 becomes

$$\chi^2 = \sum_{i=1}^{N} w(\mathbf{Q}_i)\{I_e(\mathbf{Q}_i) - [fI_c(\mathbf{Q}_i) + b]\}^2/\sigma^2. \quad (3)$$

The weight $w(\mathbf{Q}_i)$ used in (3) can be taken as the standard deviation of the experimental data or set to unity so that all points contribute equally to the summation. σ is a parameter of the modelling and controls the fraction of 'bad' moves that will be accepted. The RMC process proceeds as described in §2.2. The scaling factor f and the background parameter b are computed after each RMC move. The program allows three different operation modes:

(i) the scaling factor and background parameter can be set to fixed values;

(ii) only the scaling factor f is used and b is set to a fixed value b_0, f is then calculated according to (4*a*);

(iii) both scaling factor f and background parameter b are used. Their values are then calculated according to (4*b*).

$$f = \sum_{i=1}^{N} w(\mathbf{Q}_i) I_e(\mathbf{Q}_i) I_c(\mathbf{Q}_i) \Big/ \sum_{i=1}^{N} w(\mathbf{Q}_i) I_c^2(\mathbf{Q}_i), \quad b = b_0 \tag{4a}$$

$$\begin{aligned} f = & \left[\sum_{i=1}^{N} w(\mathbf{Q}_i) \sum_{i=1}^{N} w(\mathbf{Q}_i) I_e(\mathbf{Q}_i) I_c(\mathbf{Q}_i) \right. \\ & \left. - \sum_{i=1}^{N} w(\mathbf{Q}_i) I_e(\mathbf{Q}_i) \sum_{i=1}^{N} w(\mathbf{Q}_i) I_c(\mathbf{Q}_i) \right] \\ & \times \left\{ \sum_{i=1}^{N} w(\mathbf{Q}_i) \sum_{i=1}^{N} w(\mathbf{Q}_i) I_c^2(\mathbf{Q}_i) \right. \\ & \left. - \left[\sum_{i=1}^{N} w(\mathbf{Q}_i) I_c(\mathbf{Q}_i) \right]^2 \right\}^{-1}, \\ b = & \left[\sum_{i=1}^{N} w(\mathbf{Q}_i) I_e(\mathbf{Q}_i) - f \sum_{i=1}^{N} w(\mathbf{Q}_i) I_c(\mathbf{Q}_i) \right] \Big/ \sum_{i=1}^{N} w(\mathbf{Q}_i). \end{aligned} \tag{4b}$$

In fact, the program computes an individual scaling factor and background for each plane of experimental data. This allows one to use data sets for the RMC simulations from different experiments, *e.g.* neutron and X-ray diffuse scattering data or measurements made with different wavelengths.

The first step to run a RMC simulation is to create a starting structure. The program *DISCUS* allows various ways of setting up such a structure. The easiest is to build the structure from the contents of an asymmetric unit. The latter is expanded to the whole unit cell using the space-group symbol. *DISCUS* also provides various tools to modify the structure, *e.g.* to introduce vacancies or to apply random displacements to the atoms with mean-square amplitudes corresponding to their observed isotropic temperature factors. For further details of the program, see Proffen & Neder (1997).

The size (in unit cells) of the model crystal used is dictated by the following considerations. Firstly, the total number of unit cells should be as large as is computationally feasible in order to ensure that statistical variations within the sample do not unduly affect the results. (In previous 3D MC studies, model crystals of about 32 × 32 × 32 unit cells have proved satisfactory, while crystals significantly smaller than this have been rather too noisy.) Secondly, in order to avoid contributions to the calculated intensity due to the finite (and small) size of the simulated crystal, periodic boundary conditions should be applied. This means the size of the crystal used for the simulation and the minimal grid size $\Delta\mathbf{Q}$ of the experimental data must fulfil the following condition:

$$\Delta\mathbf{Q} = \left((1/n_a)a^*, (1/n_b)b^*, (1/n_c)c^*\right). \tag{5}$$

The values a^*, b^* and c^* are the reciprocal-lattice parameters and n_a, n_b and n_c stand for the size of the model crystal in unit cells. In this picture, the whole crystal can be seen as a 'supercell' where all experimental data points represent Bragg peaks. In those points, the distribution due to the finite size of the crystal is zero. In practice, this relation requires, for example, a crystal size of 20 × 20 × 20 unit cells, given a grid size of $\Delta Q_{h,k,l} = 0.05$ reciprocal-lattice units. This size of crystal was adopted in the present work for the 3D simulations as a reasonable compromise between the need for as large a sample size as possible and the need to obtain results in a reasonable time.

The concept of the individual MC or RMC 'move' was introduced in §2.1. In practice, we use a mode of simulation in which occupational disorder is modelled by swapping two different randomly selected atoms (Fig. 1*a*). This procedure forces the relative abundances of the different atoms within the crystal to be constant. It should be noted that vacancies are treated as an additional atom type within the program *DISCUS*. The

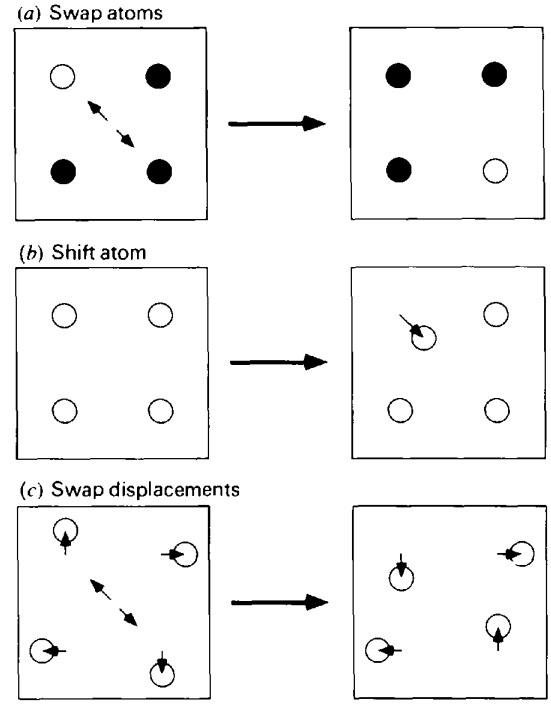

Fig. 1. Illustration of the RMC modes: (*a*) swap atoms, (*b*) shift atom and (*c*) swap displacements from average position.

introduction of displacement disorder is realized in two different ways. In the first method, a randomly selected atom is displaced by a random Gaussian distributed amount (Fig. 1*b*). Alternatively, the displacement variables associated with two different randomly selected atoms are interchanged (Fig. 1*c*). The latter method has the advantage that the overall mean-square displacement averages for each atom site can be introduced into the starting model and these will remain constant throughout the simulation. A further discussion about the different 'displacement modes' is given in §4.2. Before a RMC move is carried out, the program checks if the particular displacement would move atoms closer together than a user-defined lower limit. Those limits are set individually for all atom-type pairs. Additional information about the program *DISCUS* can be found in Proffen & Neder (1997) or on the *DISCUS* WWW homepage (Neder & Proffen, 1996).

3. Creation of 2D disordered 'test' structures

The disordered 2D test structures were created using the direct MC method described in §2.1. The starting structure was a 2D square-symmetric crystal with a size of 50×50 unit cells, one atom (Zr) on (0, 0, 0) and a lattice constant of $a = 5$ Å. Subsequently, two different MC computations were carried out to introduce occupational and displacement disorder. Binary random variables $\sigma_{i,j}$ are used to represent the atom array with $\sigma_{i,j} = +1$ to represent a Zr atom and $\sigma_{i,j} = -1$ for a vacancy. The energy of interaction between sites used in the MC vacancy-ordering scheme is of the form

$$E_{\text{occ}} = \sum_{i,j} \sigma_{i,j}[H + J_1\sigma_{\langle 10\rangle} + J_2\sigma_{\langle 11\rangle}], \qquad (6)$$

where $\sigma_{\langle 10\rangle}$ is the sum of all four nearest-neighbour variables and $\sigma_{\langle 11\rangle}$ the sum of all four next-nearest-neighbour variables. The sum in (6) is over all crystal sites i and j. The interaction parameters H, J_1 and J_2 are initially unknown and a feedback mechanism is used to achieve the desired ordering of the vacancies. The displacements were modelled in a similar way using a Hamiltonian, where the atoms move in harmonic potentials (Hooke's law).

$$E_{\text{disp}} = \sum_{i,j} k(d_{i,j} - \tau_{i,j}\, d_0)^2. \qquad (7)$$

The sum is over all atoms i and all nearest-neighbour atoms j. Only nearest-neighbour terms are used in this modelling. The atom–atom distance is given by $d_{i,j}$, the average distance is d_0, $t_{i,j}$ is the displacement factor and k a force constant.

Two different disordered structures were created showing only occupational disorder and an additional two structures using subsequent 'displacement' MC simulations. Each simulation was carried out for 100 cycles, *i.e.* every crystal site was visited 100 times on average. We will refer to the correlation coefficient (Welberry, 1985) to nearest neighbours in the $\langle 10\rangle$ direction as c_{10} and in the $\langle 11\rangle$ direction as c_{11}. The achieved vacancy concentration Θ, correlations c_{10}, c_{11} and the average nearest-neighbour distances Zr—Zr and Zr—vacancy are listed in Table 1. Structures 1 and 2 (Figs. 2*a*, *d*) show only the given occupational disorder, whereas structures 3 and 4 include additionally the given displacements. Structure 1 shows vacancy pairs preferred in the $\langle 10\rangle$ direction corresponding to the large positive correlation c_{10} in that direction. The value of c_{11} is close to its maximum negative value of $-\Theta/(1-\Theta) = -0.164$, *i.e.* only very few $\langle 11\rangle$ vacancy pairs are present in the structure. Structure 2 is characterized by a positive correlation c_{11} and a negative value for c_{10} [maximum negative value $-\Theta/(1-\Theta) = -0.205$], which results in preferred $\langle 11\rangle$ vacancy pairs and avoided $\langle 10\rangle$ pairs. Structures 3 and 4 show additional size effects like distortions (Butler & Welberry, 1993) created by shifting the nearest neighbours towards the vacancy. The Zr atoms were displaced using the MC simulation technique. The values of $\tau_{i,j}$ in the energy term [(7)] for the MC simulations were set to $\tau_{\text{Zr—Zr}} = 5.05$ Å and $\tau_{\text{Zr—vac}} = 4.85$ Å to achieve the desired displacements. Finally, all atom positions in the resulting structure were displaced by an additional random amount corresponding to an isotropic temperature factor of $B = 0.5$ Å^2 (note $B = 8\pi^2\langle u^2\rangle$). The standard deviations of the mean distances $d_{\text{Zr—Zr}}$ and $d_{\text{Zr—vac}}$ of structure 4 are slightly higher than for structure 3 as a result of the MC modelling.

Table 1. *Correlations and displacements of the two-dimensional test structures*

Structures 1 and 2 show only occupational disorder according to the given correlations. Structures 3 and 4 include the same vacancy ordering and subsequent displacements as given below.

	Structures 1/3	Structures 2/4
Concentration Θ	0.141	0.170
c_{10}	0.406	−0.203
c_{11}	−0.143	0.523
$d_{\text{Zr—Zr}}$ (Å)	5.02 (11)	5.05 (12)
$d_{\text{Zr—vac}}$ (Å)	4.89 (9)	4.90 (12)

The diffuse scattering patterns used as input for the RMC simulations are the Fourier transforms of the disordered structures described above. For all simulations, the neutron scattering patterns at a wavelength of $\lambda = 1$ Å were computed (Fig. 2). The calculated area extends from $h, k = 0.0$ r.l.u. to $h, k = 6.0$ r.l.u. with a resolution of $\Delta h, k = 0.02$ r.l.u. corresponding to the condition given in (5) for a 50×50 unit-cell crystal. The Bragg peaks were excluded in all data sets. Finally, the scattering data were multiplied with a scaling factor of $f = 0.2$ and a flat background of $b = 50.0$ was added. The diffraction pattern (Fig. 2*b*) corresponding

to structure 1 shows diffuse streaks in the [10] direction intersecting at the Bragg positions owing to the positive c_{10} correlation in the disordered structure. The scattering of structure 2 (Fig. 2*e*) shows diffuse streaks parallel to [11] and additional peaks at positions $(h/2, k/2)$ with h, k integers. These peaks can be explained by the negative correlation c_{10}, *i.e.* preferred Zr—vacancy pairs in the direction that leads to a virtual doubling of the unit cell. The diffuse scattering patterns (Figs. 2*c*, *f*) of the distorted structures show increasing diffuse intensities with increasing **Q** values, characteristic for displacement disorder. Additionally, the size-effect type of the introduced displacements causes the observed 'transfer' of diffuse intensity to the lower scattering angles across lines parallel to [10].

4. 2D simulations

All simulations were carried out on a HP 9000/735 workstation with the program *DISCUS* (Proffen & Neder, 1997). Rather than using the final χ^2 value [(3)] to compare the agreement between the observed (*i.e.* simulated) and the calculated diffuse scattering of the different runs, a weighted R value was computed. The actual values of R for the agreement of complete diffuse diffraction patterns are likely to be higher than values familiar from conventional crystal structure refinements and are used in this paper only as a method of comparing the results of different RMC refinements.

4.1. *Occupational disorder*

The first runs were carried out to model pure occupational disorder with the RMC technique starting from the diffuse scattering data (Figs. 2*b*, *e*) corresponding to structures 1 (run O1) and 2 (run O2). Scaling factor and background parameter were fixed to their initial values of $f = 0.2$ and $b = 50.0$. The weights $w(\mathbf{Q})$ for all presented simulations were set to unity for all data points. After about 24 h CPU time and a total of 15 RMC cycles, the convergence was sufficiently complete that only a much longer run time would lead to small further changes in the structure. The refinement was stopped at that stage. The correlations achieved and the R values of runs O1 and O2 are listed in Table 2. In order to avoid local minima, the parameter σ was adjusted to allow a reasonable proportion (~5–10%) of accepted 'bad'

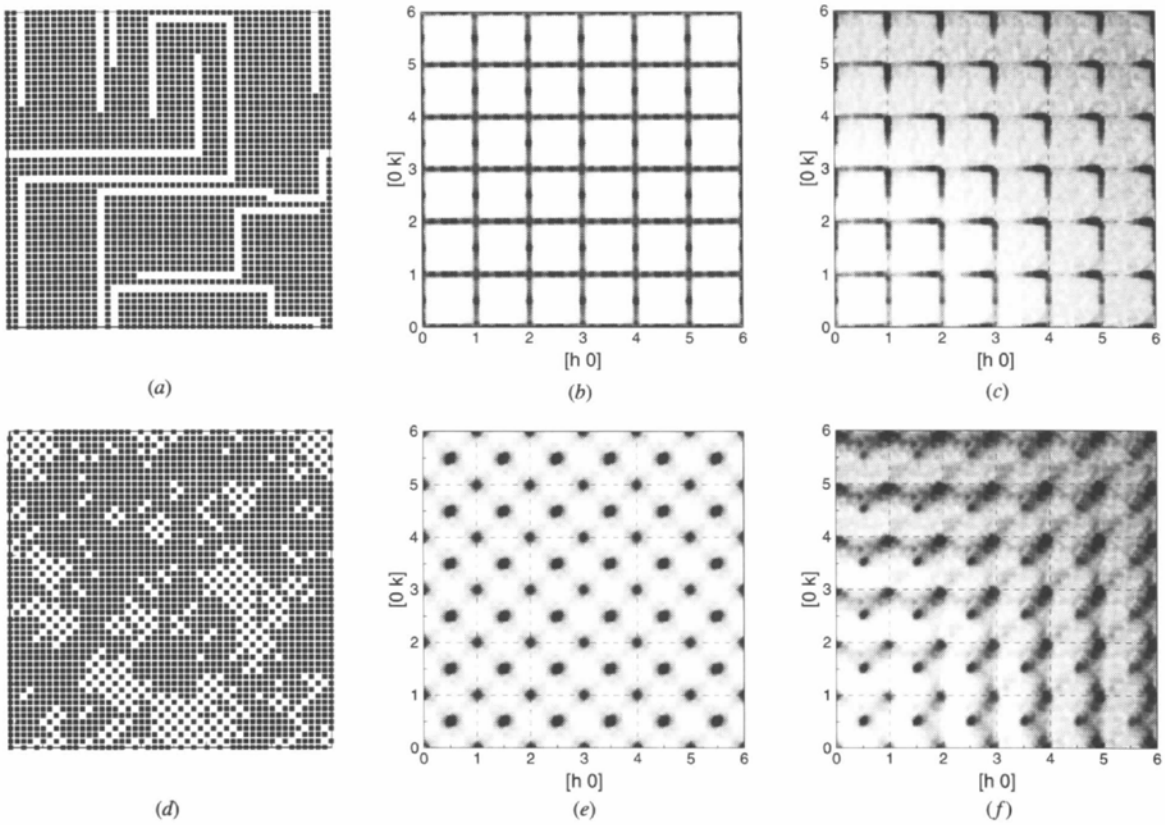

Fig. 2. Simulated disordered structures and diffuse scattering intensities. (*a*) Structure 1 showing preferred ⟨10⟩ vacancy pairs, correlations $c_{10} = 0.506$, $c_{11} = -0.143$. (*b*) Calculated diffraction pattern for structure 1. (*c*) Calculated diffraction pattern for structure 3. (*d*) Structure 2 showing preferred ⟨11⟩ vacancy pairs, correlations $c_{10} = -0.203$, $c_{11} = 0.523$. Calculated diffraction pattern for (*e*) structure 2 and (*f*) structure 4. The intensity scale for images (*b*) and (*e*) is enlarged by a factor of 2 compared with (*c*) and (*f*).

Table 2. *Results of RMC occupational refinement runs O1 and O2 (see text)*

	Structures 1/3	Structures 2/4
c_{10}	0.270	−0.174
c_{11}	−0.109	0.455
R (%)	18.6	16.1

Table 3. *Results of RMC displacement refinement runs D1 to D3 (see text)*

	Run D1	Run D2	Run D3
d_{Zr-Zr} (Å)	5.02 (9)	5.02 (14)	5.02 (15)
d_{Zr-vac} (Å)	4.96 (9)	4.97 (15)	4.97 (14)
R (%)	35.2	28.4	37.4

moves. The resulting structures and diffraction patterns of refinements O1 and O2 are shown in Fig. 3. The calculated diffuse intensities (Figs. 3*a*, *b*) show good agreement with the observed data. The defect structures obtained (Figs. 3*c*, *d*) contain the correct type of occupational disorder, *i.e.* ⟨10⟩ vacancy pairs for run O1 and ⟨11⟩ pairs for run O2. The correlation values achieved, however, show residual differences from the correlations of the corresponding input structures, mainly reflecting the small number of remaining single vacancies (Figs. 3*c*, *d*). Further RMC cycles might sightly improve the agreement between those values.

4.2. *Displacements*

In this second series of simulations, the size-effect-like distortions were modelled. As the input data (Figs. 2*c* and *f*) corresponding to structures 3 and 4 show occupational and displacement disorder, the appropriate vacancy ordering was included in the starting structure for the RMC calculations and only the distortions were refined. The atoms in the starting structures were given displacements corresponding to an isotropic temperature factor of $B_{Zr} = 0.5\,\text{Å}^2$. Run D1 was carried out using the 'swap-displacements' mode (Fig. 1*c*) whereas run D2 represents a similar simulation using the plain 'shift' mode (Fig. 1*b*). The introduced shifts followed a Gaussian distribution with a half-width of 0.05 Å. The minimum allowed distance between Zr atoms was set to 4.7 Å. Scaling factor and background were again fixed to their theoretical values. As for the previous runs, the RMC simulations were stopped after 15 RMC cycles, when the refinement showed only very slow further progress. The displacements achieved and resulting R values are summarized in Table 3. Run D2 using the 'shift' mode shows a better R value compared with run D1. Inspection of the calculated diffraction patterns (Figs. 4*a*, *b*) reveals that the total diffuse scattering at high **Q** vectors shows a better agreement for the 'shift' mode run D2 (Fig. 4*b*). The resulting nearest-neighbour distances Zr—Zr and Zr—vacancy, however, are sim-

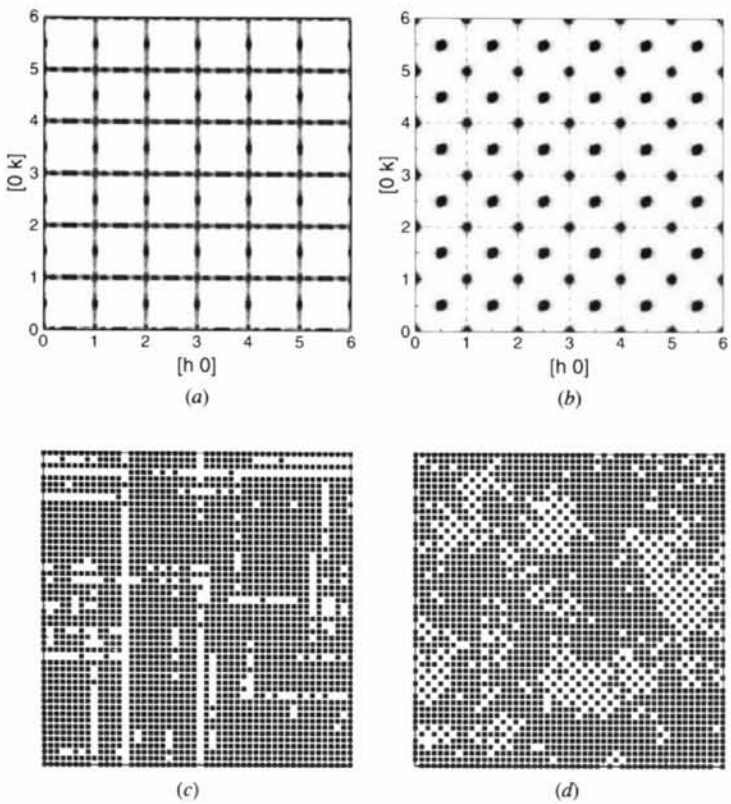

Fig. 3. Results of RMC refinements. Calculated diffuse scattering for (*a*) run O1 and (*b*) run O2 and resulting structures of (*c*) run O1 and (*d*) run O2.

ilar for both runs, whereas their standard deviation is larger for the 'shift' mode simulation. The mean-square displacements produced by simulation D1 show good agreement with the expected value according to the temperature factor. The corresponding bond-length distributions (Fig. 5) reveal that run D2 ('shift' mode) resulted in a set of displacements not consistent with the model structure. The distribution for run D2 is too broad and especially the additional peak near the cutoff at a bond length of 4.7 Å, marked by an arrow in Fig. 5(*b*), is not present in the bond-length distribution of the input structure (Fig. 5*c*). The results of these simulations favour the 'swap-displacements' mode, which allows the initial mean-square displacements present in the starting structure to be maintained and leads to plausible bond-length distributions. As for the occupational disorder results, the main disorder element (atoms move toward the vacancies) is produced correctly by the RMC refinements. However, in all RMC runs the resulting displacements are smaller than the expected values from the input structures (Table 1).

The diffraction patterns used for these simulations (Figs. 2*c* and *f*) are dominated by displacement diffuse scattering contributions. An additional simulation (D3) was carried out starting from a random vacancy distribution, *i.e.* the diffuse scattering data including occupational disorder as well as distortions were modelled only by displacements. 15 RMC cycles were computed using identical settings to run D2. The resulting displacements and R values are included in Table 3. The

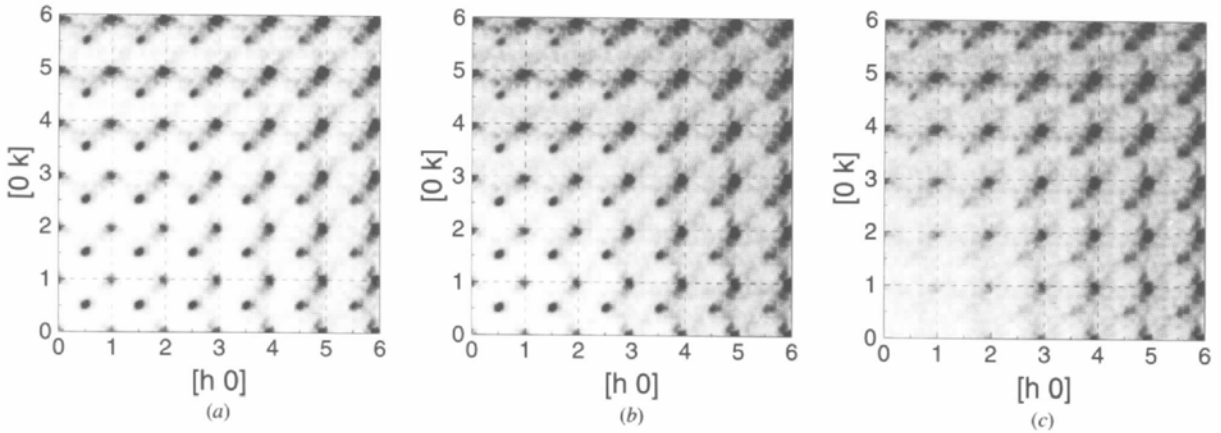

Fig. 4. Calculated diffuse scattering patterns for: (*a*) RMC run D1 using the swap-displacements mode; (*b*) run D2 using the shift mode; and (*c*) run D3 (for details see text).

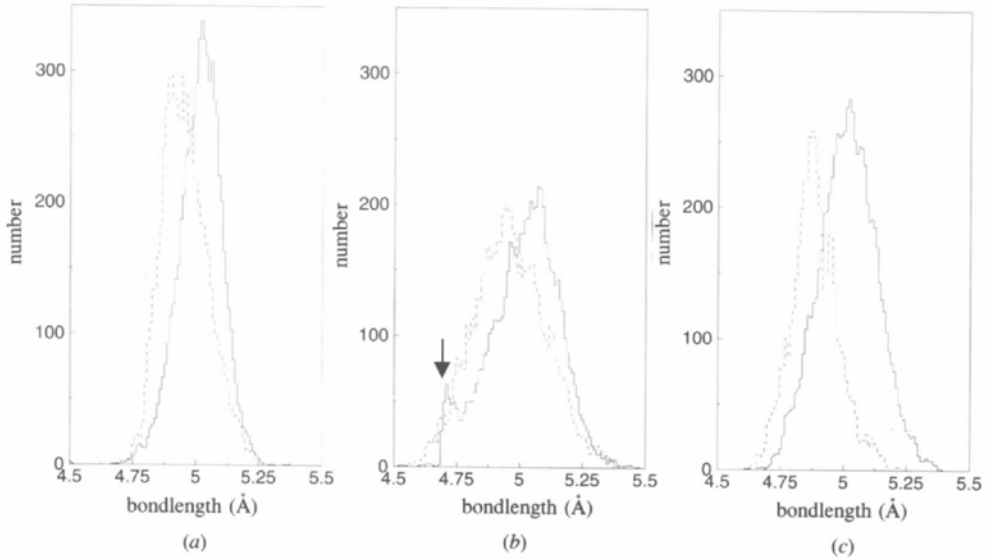

Fig. 5. Bond-length distributions for nearest-neighbour distances Zr—Zr (solid line) and Zr—vacancy (dashed line, enlarged by a factor of 4): (*a*) RMC run D1 using the swap-displacements mode; (*b*) RMC run D2 using the shift mode; (*c*) test structure used to calculate the input data (for details see text).

final R value of this run is higher compared with the value reached in run D2. The mean distances for Zr—Zr and Zr—vacancy are consistent with the size-effect-like distortions of the input structure. Inspection of the resulting diffraction pattern (Fig. 4*c*) reveals that significant diffuse features due to the occupational disorder at low **Q** values are absent from the calculated pattern. The agreement at higher **Q** values, however, is of comparable quality to the results of run D2, which included the occupational disorder. This result points out the importance of sufficient experimental data covering a large range of **Q** space.

4.3. *Combination of occupational and displacement disorder*

The previous simulations show that occupational as well as displacement disorder can be individually well modelled using the RMC simulation technique. However, the crucial question remains as to whether it is possible to get information about the chemical ordering from a system showing occupational disorder and displacements. To answer this question, a series of RMC simulations based on the diffuse scattering data from structures 3 and 4 (Figs. 2*c*, *f*) was carried out. All runs started from a structure showing a random vacancy distribution and displacements corresponding to an isotropic temperature factor of $B = 0.5$ Å^2. Scaling factor and background were fixed at $f = 0.2$ and $b = 50.0$ as in the previous simulations. Simulations C1 and C1′ were carried out by alternately executing one cycle in 'swap-atoms' mode followed by one cycle in 'swap-displacements' mode. In the first cycle, the parameter σ was set to a value to allow a relative abundance of about 6% 'bad' moves of all accepted moves. The value of σ was linearly decreased in each successive cycle so that in the last cycle only moves that improved the refinement were accepted. 15 cycles of each RMC mode were computed consuming about 60 h CPU time. The resulting correlations, displacements and R values are listed in Table 4. Comparing the results for the displacements of run C1′ and run D1 shows that the final distortions are of the same size as for the previous runs where the occupational disorder was given in the starting structure. In simulation C1, the direction of the displacements is parallel to the direction of the positive correlation, whereas the direction of the displacements in run C1′ coincides with direction of the negative correlations. Refinement C1 (Table 4) shows the expected positive correlation in the ⟨10⟩ direction as well as a positive correlation in the ⟨11⟩ direction where a negative value was expected. The resulting structure (Fig. 6*d*) shows that the vacancies

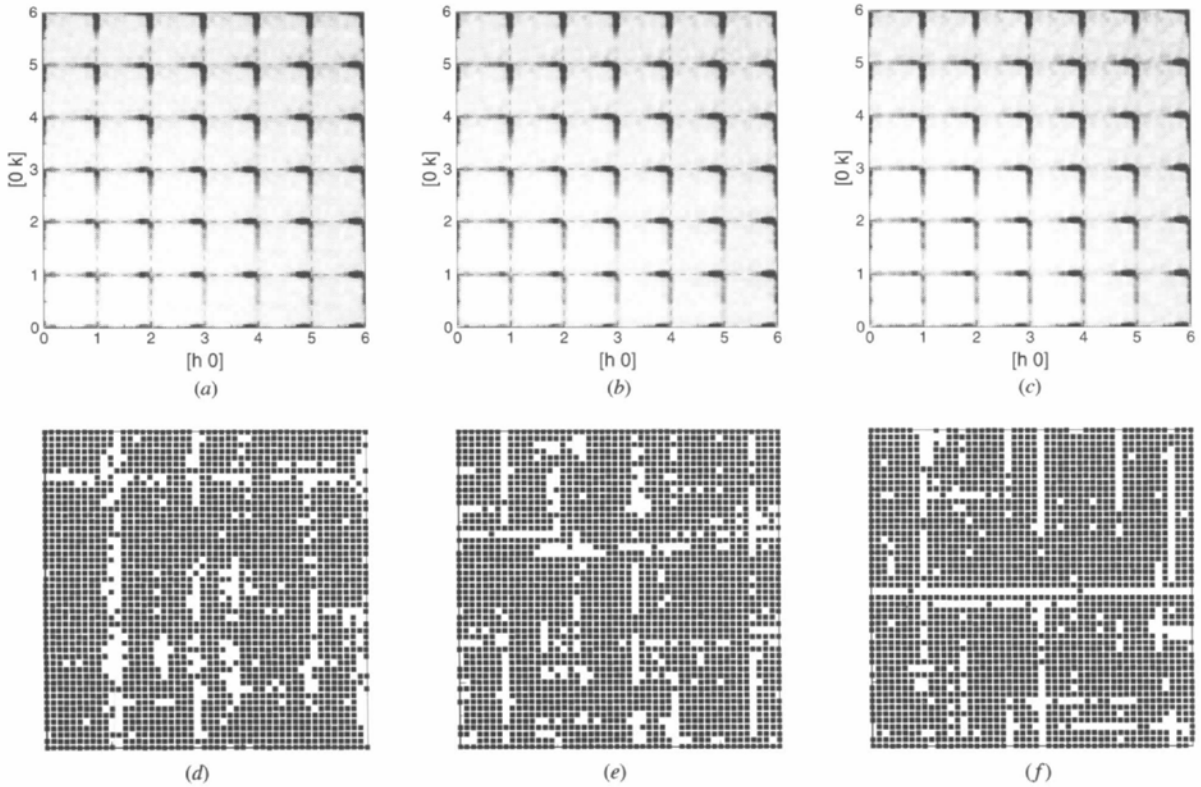

Fig. 6. Results of RMC refinements. Calculated diffraction patterns: (*a*) run C1, (*b*) run C2 and (*c*) run C4; and resulting structures for runs (*d*) C1, (*e*) C2 and (*f*) C4.

Table 4. *Results of the RMC refinement runs*

(*a*) C1 to C4

	Run C1	Run C2	Run C3	Run C4
c_{10}	0.311	0.279	0.215	0.287
c_{11}	0.164	0.011	−0.015	−0.052
$d_{Zr—Zr}$ (Å)	5.01 (9)	5.01 (8)	5.01 (9)	5.01 (9)
$d_{Zr—vac}$ (Å)	4.96 (12)	4.95 (10)	4.97 (11)	4.95 (10)
R (%)	26.5	21.5	23.8	22.3

(*b*) C1′ to C4′

	Run C1′	Run C2′	Run C3′	Run C4′
c_{10}	0.188	0.044	0.002	−0.076
c_{11}	0.290	0.278	0.270	0.412
$d_{Zr—Zr}$ (Å)	5.02 (9)	5.02 (9)	5.02 (8)	5.02 (8)
$d_{Zr—vac}$ (Å)	4.95 (11)	4.96 (10)	4.97 (10)	4.97 (10)
R (%)	39.3	36.4	38.7	39.2

are clustered together rather than forming long separate chains along ⟨10⟩ as in the corresponding input structure (Fig. 2*a*). The calculated diffraction pattern (Fig. 6*a*) shows a good agreement except for a high level of broad diffuse scattering at low **Q** values not present in the experimental data. The poor agreement between observed and calculated diffuse scattering at low **Q** values is even more pronounced in the result of run C1′ (Fig. 7*a*). The diffuse intensity at positions $(h/2, k/2)$, with h and k integers, are mainly caused by the vacancy ordering. In the resulting diffraction pattern of run D3 (Fig. 4*c*) showing no vacancy ordering, those features are completely absent. The final structure of run C1′ (Fig. 7*d*) shows positive correlations in the ⟨10⟩ and ⟨11⟩ directions (Table 4) and subsequently the calculated diffuse scattering at low **Q** values shows poor agreement with the input data. It appears that the dominant part of the diffuse scattering caused by the displacements has too strong an influence on the correlations that are achieved.

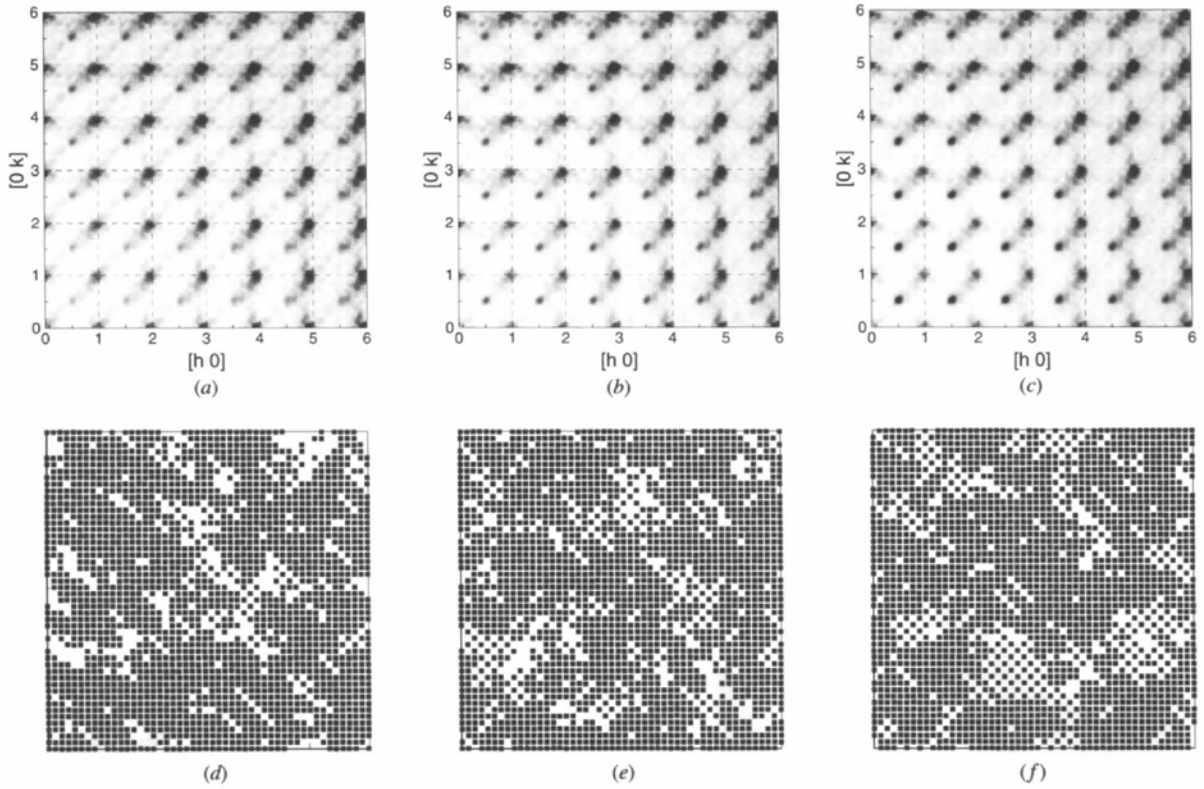

Fig. 7. Results of RMC refinements. Calculated diffraction patterns: (*a*) run C1′, (*b*) run C2′ and (*c*) run C4′; and resulting structures for runs (*d*) C1′, (*e*) C2′ and (*f*) C4′.

In order to model both parts of the defect structure more simultaneously, during refinements C2 and C2′ the 'swap-atoms' and 'swap-displacements' modes were alternated every 0.1 cycles, *i.e.* the number of moves necessary to visit 10% of all atom sites on average. This procedure was an attempt to avoid the possibility that a particular vacancy ordering, unduly influenced by displacement diffuse scattering contributions, 'freezes in' during the first cycle. All other settings were identical to those of refinements C1 and C1′. The results listed in Table 4 show a significant improvement of the R values compared with the previous runs. The resulting displacements are similar to the values of the previous refinements and seem to be relatively insensitive to the way both RMC modes are alternated during the refinement. In contrast, the correlation values achieved show a significant change. In the directions of the expected negative correlations, the values achieved are close to zero. The positive correlations are smaller than in the previous run. However, the observed and calculated diffuse scattering at low **Q** vectors (Figs. 6*b* and 7*b*) are in better agreement. The final structures (Figs. 6*e* and 7*e*) show less 'clustering' of the vacancies than in the previous runs. Additional test refinements where the two RMC modes were alternated after each single move brought no further improvement.

The main problem in achieving a better modelling of the occupational disorder is the fact that the vacancy ordering reaches its final configuration after about 4 cycles. At this stage, the diffuse scattering distribution due to displacements is still not large enough to avoid a strong influence on the 'swap-atoms' part of the refinement. A solution might be to allow initially a large amount of 'bad' moves during the 'swap-atoms' cycles to allow later changes of the vacancy ordering. On the other hand, one has to make sure that occupational changes and displacements are able to reach a final minimum. Refinements C3 and C3′ were done allowing a relative abundance of 50% 'bad' moves in the first cycle down to 1% in the final cycle. All other settings are identical to those of the previous refinements C2 and C2′. The calculated diffraction patterns and the resulting structures (not displayed here) are similar to the results of the previous runs C2/C2′. The final R values (Table 4) are slightly higher than in the previous refinement, but it is likely that this is caused by the large number of 'bad' moves accepted during the refinement. Refinement C3 even achieved a small negative value for c_{11} (Table 4). It should be noted that the expected positive correlations are also smaller compared with the previously achieved values. So far, the improvements of the expected negative correlations lead to a worsening of the positive correlations. The resulting displacements have similar values compared with the results of the other runs.

As an alternative approach to model the vacancy ordering, the data set used for the 'swap-atoms' moves was limited to a range of $|\mathbf{Q}| < 4.0$ r.l.u., *i.e.* only the low-angle part, less affected by diffuse scattering due to distortions, was used to refine the vacancy ordering. The part of the refinement modelling the displacements used the complete data sets. The parameter σ was returned to the old value, allowing initially 6% 'bad' moves. Optical inspection of the calculated diffraction patterns (Figs. 6*c* and 7*c*) shows the best agreement with the input data set, especially the diffuse scattering at low **Q** values is much better modelled than in the other refinements, although the R values (Table 4) are worse compared with the previous runs. However, the resulting structures (Figs. 6*f* and 7*f*) and correlation values achieved (Table 4) give the best description of the simulated disordered structures.

4.4. *Experimental factors*

So far, the diffuse scattering used for the RMC refinements was calculated from the Fourier transform of simulated structures and the known values for the scaling factor f and (flat) background b were kept fixed in the refinements. In this section, the influence of factors like scaling factor, a noisy background or rebinning of the input data will be studied. All refinements were carried out the same way as in run C4, *i.e.* using only low-**Q** data for the occupational moves and alternating 'swap atoms' and 'swap displacements' every 0.1 cycles.

The first refinement (E1) uses (4*b*) to calculated scaling factor f and background parameter b after each RMC move. The correlations achieved, displacements and the final values of the scaling factor f and background b are listed in Table 5. Compared with refinement C4 with f and b fixed to their expected values, the final correlation c_{10} is smaller in run E1, whereas the value for c_{11} is slightly more negative. Inspection of the calculated diffraction pattern and the resulting structure (Figs. 8*a* and *d*) reveals a comparable result for both refinements. Although one could expect a correlation between the scaling factor and the size of the achieved distortions, the final displacements are of the same size as in the corresponding run using a fixed scaling factor. However, the size of the resulting distortions is still smaller than the shifts in the input structure. The better R value for the refinement E1 is most likely caused by the slightly larger scaling factor of $f = 0.28$ compared with the expected value of $f_0 = 0.20$. The resulting background parameter $b = 47.8$ is very close to the theoretical background of $b_0 = 50.0$.

As additional experimental influence, the flat background, $b = 50.0$, of the input data was replaced by a noisy background. The new background was generated by $b = b_0 + G$, where $b_0 = 100.0$ is a constant offset and G is a Gaussian distributed random number. The half-width of the distribution was FW = 45.0. A cross section of the experimental data along h at $k = 0.74$ r.l.u. with the flat as well as the noisy background can be seen in Fig. 9. Starting from this new data set, a refinement

(E2) similar to the previous one was carried out. The results are listed in Table 5; Fig. 8 contains the calculated diffuse scattering distribution (*b*) and the final structure (*e*). The higher and noisy background, clearly visible in Fig. 8(*b*), had no significant influence on the resulting defect structure. The value of c_{10} is slightly smaller than the value of run E1 (flat background) and the correlation c_{11} is a little larger than the previous value. The resulting displacements are similar to the values reached in the other RMC refinements. The calculated background parameter of $b = 93.8$ is close to the constant part $b_0 = 100.0$ of the simulated background. Although the signal-to-noise ratio at low $\mathbf{Q}$ ($|\mathbf{Q}| < 4.0$ r.l.u.) was about 4:1, the RMC simulations were able to produce a structure containing the correct vacancy ordering and distortions. The *R* value for this refinement is comparable with the previous run where the data were only affected by a flat constant background.

The minimal required size of a model crystal given by the resolution of the measured diffuse scattering data is often too large even for modern computers. Thus, the experimental data have to be rebinned to a coarser grid size. The rebinning was done by averaging all pixels falling in one element of the coarser grid. The influence of the crystal size and data rebinning is studied in the next refinement run (E3). The experimental input data with the flat background $b = 50.0$, showing a resolution of $\Delta q = 0.02$, were transformed to a grid with a size of $\Delta q = 0.05$. Subsequently, the minimal crystal size changes to 20×20 unit cells [(5)]. The coarser grid size can be clearly seen in the resulting diffuse scattering pattern (Fig. 8*c*). The achieved correlations and displacements (Table 5), however, are in good agreement with the results of the refinements using the larger crystal size. The rebinning of the data results in a change of the scaling factor *f*. In contrast to the previous runs, the final background parameter $b = 62.9$ is higher than the expected value of $b = 50.0$. The rebinning of the experimental data had no significant influence on the results achieved by the RMC modelling for this system. However, it is important to make sure that the measured diffuse scattering distribution is broad enough for the particular grid size to be used in the modelling.

5. 3D simulations

The two-dimensional refinements described in the last section used a 'complete' diffuse scattering data set up to a maximum $\mathbf{Q}$ as input. In three dimensions, it is often impossible to use a 'complete' 3D data set owing to time-consuming diffuse scattering data collections and limited computer resources. For the 3D refinements presented in this chapter, a disordered model crystal was created using MC simulations similar to the 2D case

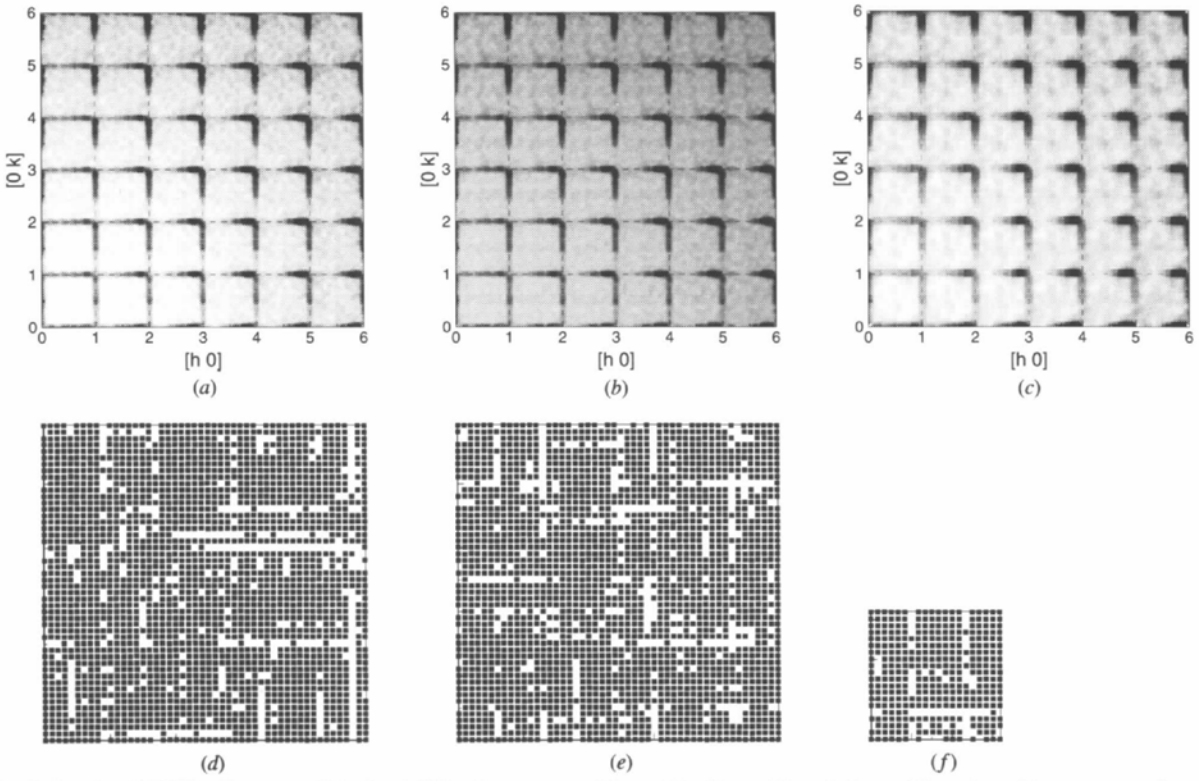

Fig. 8. Results of RMC refinements. Calculated diffraction patterns: (*a*) run E1, (*b*) run E2 and (*c*) run E3; and resulting structures for runs (*d*) E1, (*e*) E2 and (*f*) E3.

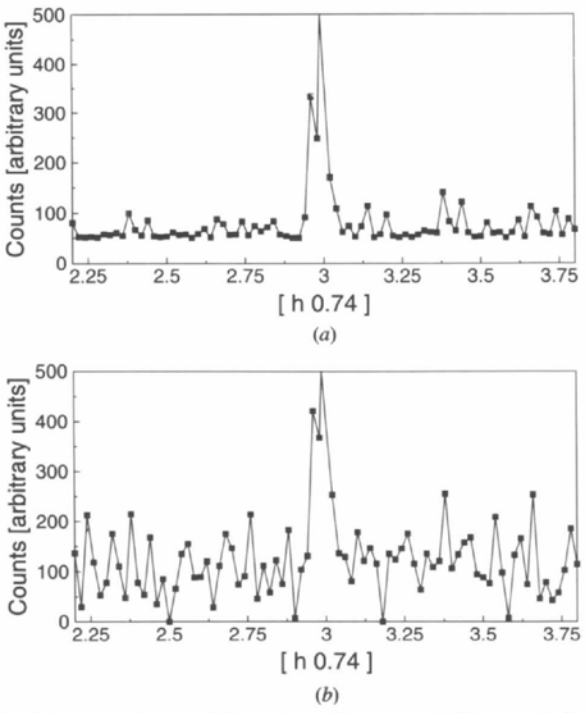

Fig. 9. Cross section parallel to h at $k = 0.74$ r.l.u. of diffuse scattering input data: (*a*) with a flat background at $b = 50.0$ and (*b*) with a noisy background used for run E2.

Table 5. *Results of the RMC refinement runs E1 to E3*

	Run E1	Run E2	Run E3
c_{10}	0.208	0.190	0.223
c_{11}	−0.067	−0.042	−0.050
$d_{Zr—Zr}$ (Å)	5.01 (9)	5.01 (9)	5.01 (8)
$d_{Zr—vac}$ (Å)	4.96 (10)	4.97 (11)	4.96 (10)
f	0.28	0.28	1.43
b	47.8	93.8	62.9
R (%)	21.4	24.6	23.5

(see §3). The size of the cubic crystal is $20 \times 20 \times 20$ unit cells with a lattice constant of $a = 5$ Å containing Zr on $(0, 0, 0)$. The crystal contains 15.7% vacancies on the Zr sites showing a positive correlation in $\langle 100 \rangle$ directions and negative correlations in $\langle 110 \rangle$ and $\langle 111 \rangle$ directions. The correlation values and displacements are listed in Table 6. As for the 2D structures, the atoms are relaxed towards the vacancies (size effect). The resulting disordered structure was finally displaced according to the isotropic temperature factor $B = 0.5$ Å^2. As input for the RMC simulations, experimental data planes with nc^* ($n = 0.0, 0.5, 1.0, \ldots, 4.0, 5.0, 6.0$) from $h, k = 0.0$ r.l.u. to $h, k = 6.0$ r.l.u. containing 121×121 data points were calculated using neutron scattering at a wavelength of $\lambda = 1$ Å. Bragg peaks were excluded from the RMC input data. The corresponding grid size of $\Delta q = 0.05$ fulfils (5) for the given crystal size. The data were scaled

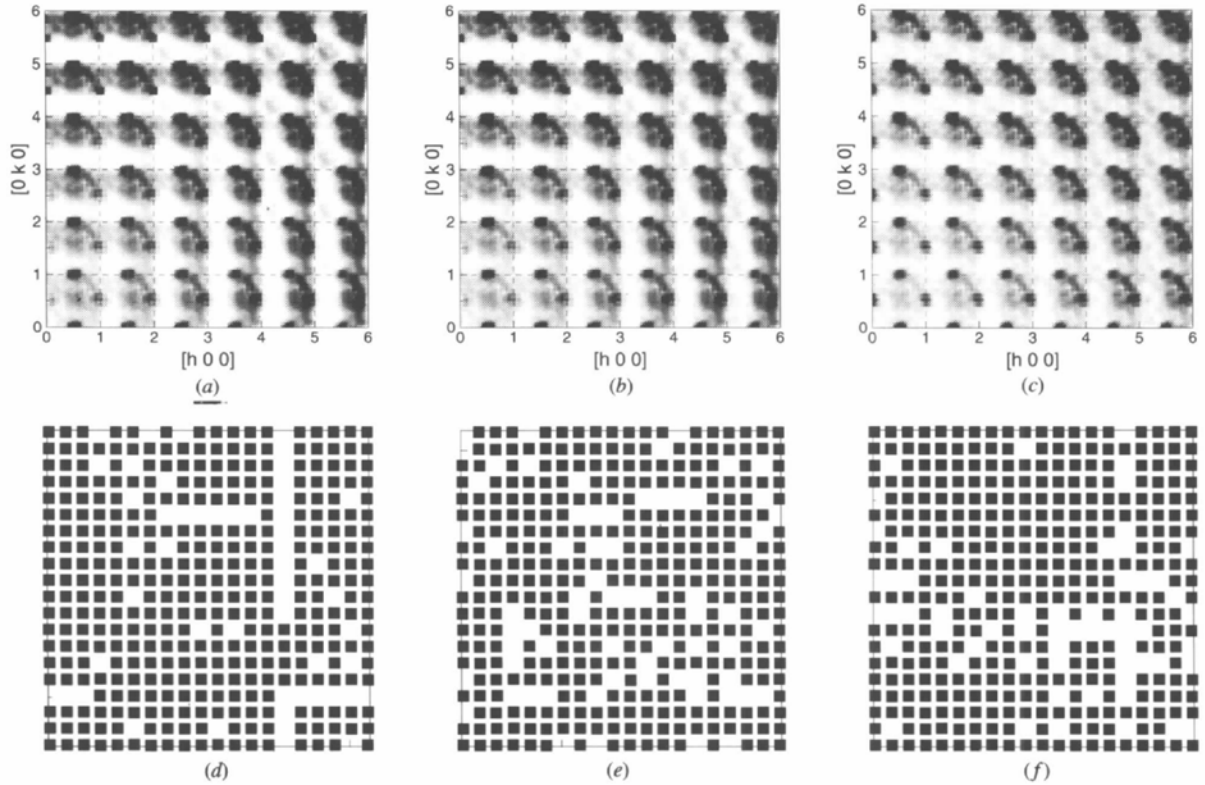

Fig. 10. 3D RMC refinements. Diffraction pattern of layer $0.0c^*$ of (*a*) starting structure, (*b*) results of run V1 and (*c*) run V2. The $xy0$ layer of the starting structure is shown in (*d*), (*e*) is the resulting structure of run V1 and (*f*) run V2.

by a factor $f = 0.2$ and a flat background $b = 50.0$ was added. The diffraction pattern for the layer $0c^*$ and the $xy0$ layer of the structure are displayed in Figs. 10(*a*) and (*d*), respectively.

The first refinement (V1) was carried out using the diffraction data of the Bragg layers $0c^*$, $1c^*$ up to $6c^*$. The weights $w(\mathbf{Q})$ [(3)] were set to unity for all data points. Similar to run C4, the 'swap-atoms' and 'swap-displacements' moves were alternated every 0.1 RMC cycles. The range of data used to refine the occupational disorder was limited to $|\mathbf{Q}| < 4.0$ r.l.u.. The parameter σ was adjusted during the refinement in a way that about 6% 'bad' moves were allowed in the first cycle down to accepting no 'bad' moves in the last cycle. Scaling factor and background parameter were kept fixed at $f = 0.2$ and $b = 50.0$. Ten RMC cycles were computed lasting about 90 h CPU. Additional RMC cycles would have achieved only very small improvements of the goodness of fit without significantly changing the correlations or distortions achieved. Table 6 contains the final results after ten cycles. The calculated diffuse scattering patterns of layer $0c^*$ (Fig. 10*b*) as well as the scattering of all other layers not displayed here show a similar good agreement with the experimental data. The value listed in Table 6 is the total R factor for all used data sets. The individual R values for each single data plane range from 4.2 up to 7.7%. The $xy0$ layer of the resulting structure is displayed in Fig. 10(*e*) and shows the expected vacancy chains along $\langle 100 \rangle$. As the representation in Fig. 10(*e*) is only a 2D cross section of the structure, vacancy chains along $\langle 001 \rangle$ appear as single vacancies where the chains intersect the displayed plane of the structure. The correlations achieved (Table 6) also reflect the expected occupational disorder, *i.e.* positive correlation along $\langle 100 \rangle$ and negative correlations along $\langle 110 \rangle$ and $\langle 111 \rangle$. The absolute correlations, however, show significant differences from the expected values. The resulting shifts are consistent with the displacement disorder in the model crystal, the nearest-neighbour distance $d_{\mathrm{Zr—vac}}$ is shorter than the average distance of 5 Å, whereas the distance $d_{\mathrm{Zr—Zr}}$ is slightly longer. But, as for the correlation values, the size of the shift reached is smaller compared with the input defect structure.

Table 6. *3D RMC simulations: input structure and results of runs V1 and V2*

	Input structure	Run V1	Run V2
c_{100}	0.236	0.044	0.086
c_{110}	−0.134	−0.032	−0.089
c_{111}	−0.185	−0.045	−0.117
$d_{\mathrm{Zr—Zr}}$ (Å)	5.03 (11)	5.01 (10)	5.01 (10)
$d_{\mathrm{Zr—vac}}$ (Å)	4.92 (9)	4.98 (10)	4.98 (10)
R (%)	–	6.8	36.2

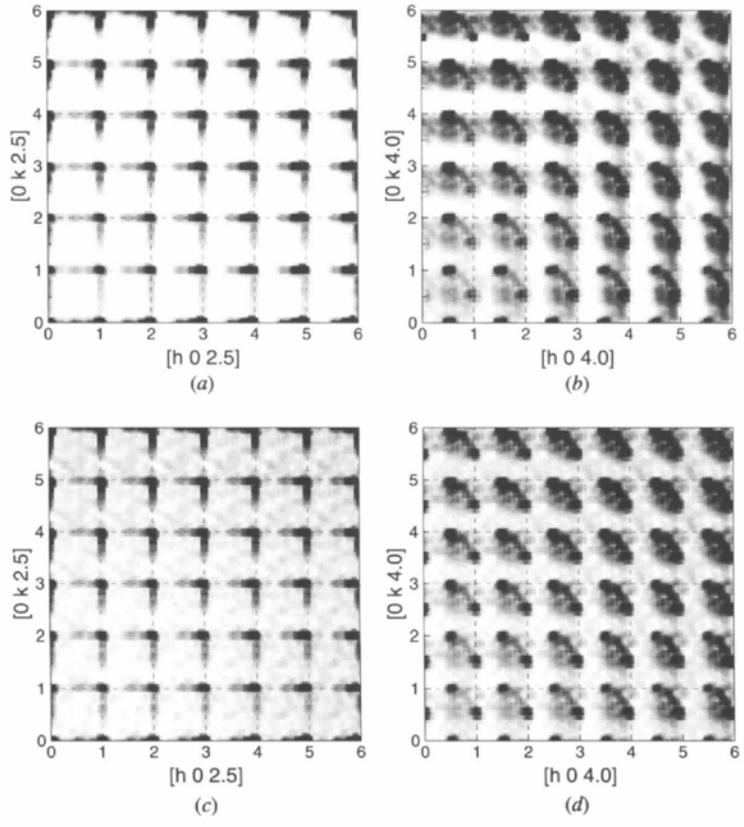

Fig. 11. 3D RMC refinements. Diffraction pattern of layer $2.5c^*$ of (*a*) starting structure and (*b*) result of run V2 showing the best individual R factor, and layer $4.0c^*$ of (*c*) starting structure and (*d*) result of run V2 showing the worst individual R factor. The image scale of images (*a*) and (*c*) are enlarged by a factor of 2 compared with (*b*) and (*d*).

Further improvement of the 3D RMC simulation results is expected using a larger set of input scattering data. For the second RMC refinement (V2), nine diffuse scattering data planes were used, corresponding to the layers $0.0c^*$, $0.5c^*$, ..., $4.0c^*$. Additionally, the cubic symmetry of the crystal was taken into account using all three symmetrically equivalent [100] planes, *i.e.* [100], [010] and [001], of each layer as input. This results in an effective number of 27 data sets used for this refinement. The RMC calculations showed a satisfactory convergence after six cycles and the simulation was stopped at that stage requiring over 200 h CPU time. The correlations and displacements achieved after run V2 are listed in Table 6. All calculated diffuse scattering planes show a similar agreement with the experimental data resulting in individual R values ranging from 31.1% for layer $2.5c^*$ up to 45.3% for layer $4.0c^*$. The observed and calculated diffraction patterns for both layers showing the smallest and largest individual R factor are displayed in Fig. 11. The high R value for layer $4.0c^*$ is mainly caused by differences of diffuse scattering intensities at high **Q** values. This indicates difficulties for the RMC refinement to achieve large enough displacements compared with the input structure (Table 6). Compared with the previous run, this refinement resulted in a slightly worse agreement between observed and calculated diffuse scattering intensities, *e.g.* see Fig. 10(*c*) for layer $0.0c^*$ of the input structure and the results of runs V1 and V2. This is reflected by the much larger R value for this refinement compared with run V1 (Table 6). However, the correlations achieved show a significant improvement (Table 6) towards the correlations of the input structure. The final distortions are similar to the results of the previous run V1. Refinement V1 was able to produce a better 'fit' based on a smaller data set. But it is important to point out that the limited range of experimental data resulted in a worse modelling of the input structure. The $xy0$ layer of the final structure of simulation V2 is shown in Fig. 10(*e*).

The 3D simulations presented here point out the importance of a sufficiently large diffuse scattering data set as input for RMC refinements. A further improvement of the presented 3D RMC simulations could be expected using even larger data sets up to complete 3D data (spacing of the data planes equal to the grid size within the planes of $\Delta h,k,l = 0.05$ r.l.u.) requiring more computer resources than feasible for these 'test' simulations.

6. Discussion

The simulation results presented in this paper indicate that the RMC simulation technique is a powerful tool to analyse diffuse scattering and to obtain information about the defect structure even of quite complex systems showing both occupational and displacement disorder. However, it is important to keep in mind that the RMC method produces one possible configuration that is consistent with the experimental data. The reported test simulations show that the resulting defect structure frequently depends on details of the refinement configuration and even more importantly on the size of the experimental data set used. It must be the aim of every RMC refinement to produce structures that are plausible from a chemical point of view. One basic requirement is to avoid configurations containing too short bond lengths. This is achieved by introducing a shortest allowed bond length for every pair of atom types present in the crystal. Every RMC move that leads to a configuration with a shorter atom–atom distance is rejected. Including a minimal distance in the RMC calculations prevents atoms from getting too close, but refinement D2 shows that simply shifting the atoms can result in unlikely bond-length distributions. An alternative approach to model displacement disorder was presented in the 'swap-displacements' mode. The starting structure for the RMC calculations is displaced according to the temperature factors of the atoms. Subsequent swapping of the displacements of two crystal sites will introduce distortions, but the mean-square displacements over the complete crystal remain constant (run D1). The problem of mean-square displacements not consistent with results of other experiments was also reported by Nield *et al.* (1995), who suggest a simultaneous refinement of diffuse and Bragg scattering to solve this problem. Our approach allows the use of known thermal parameters to create initial mean-square displacements in the model structure that will be unaffected by the RMC process. The modelling of pure occupational or displacement disorder worked straight forwardly whereas systems showing chemical disorder and distortions need more attention. All simulations of such systems (§4.3) revealed consistent displacements with the given input structure. The dominant diffuse scattering contribution due to the displacement disorder has a strong influence on the modelling of the occupational disorder. The presented simulations indicate that the alternating interval between occupational RMC moves and displacement moves is an important modelling parameter. Refinements where occupational shifts and displacements shifts are carried out alternately with no more than 10% of the crystal being visited before switching between the two modes produced the best results. Additionally, the restriction of the experimental data set to low **Q** values for the occupational RMC refinements gave a further improvement of the resulting correlations. Another important conclusion from the presented simulation results is the necessity of sufficient diffuse scattering data for the RMC modelling. The 3D RMC refinements showed a significant improvement after more diffuse scattering data were used as input. It might even be necessary to include data sets showing no diffuse scattering to improve a refinement. Having the results of this work in mind, future successful RMC refinements of the diffuse

scattering of CSZ's will mainly depend on two factors: good-quality diffuse scattering data covering large areas of reciprocal space and sufficient computer resources.

The main advantages of the direct MC method compared with other treatments of diffuse scattering including the RMC modelling technique are that it allows one to obtain a more physical picture of the disordered structure and additionally a systematic exploration of different possible causes of the observed diffuse scattering. However, in practice, it can be rather difficult to modify the real-space model crystal in a way that the 'match' with the measured diffuse scattering improves. The RMC method, on the other hand, proved to be able to reveal the defect structure from the diffuse scattering data; absolute values for correlations and displacements, however, showed remaining differences from the expected values in the 'test' structures used. The authors believe that the RMC technique is a viable method of obtaining information about the defect structure even of more complex systems showing both chemical and displacement disorder. Especially in cases where not all the observed diffuse scattering features can be described by the real-space computer model using the MC method and a further improvement of the model turns out to be difficult, the combination of MC and RMC techniques can give a further insight into the particular problem.

The authors thank D. A. Keen for many useful discussions about the RMC modelling technique. This work was supported in part by funds of the DFG (grant no. Pr 527/1-1).

References

Butler, B. D. & Welberry, T. R. (1993). *Acta Cryst.* A**49**, 736–743.

McGreevy, R. L. & Pusztai, L. (1988). *Mol. Simul.* **1**, 359–367.

Metropolis, N., Rosenbluth, A. W., Rosenbluth, M. N., Teller, A. H. & Teller, E. J. (1953). *J. Chem. Phys.* **21**, 1087–1094.

Montfrooij, W., McGreevy, R. L., Hadfield, R. & Anderson, N. H. (1996). *J. Appl. Cryst.* **29**, 285–290.

Neder, R. B., Frey, F. & Schulz, H. (1990). *Acta Cryst.* A**46**, 792–798.

Neder, R. B. & Proffen, Th. (1996). *DISCUS* Version 2.02, http://rschp2.anu.edu.au:8080/proffen/discus/discus.html.

Nield, V. M., Keen, D. A., Hayes, W. & McGreevy, R. L. (1992). *J. Phys. Condens. Matter*, **4**, 6703–6714.

Nield, V. M., Keen, D. A., Hayes, W. & McGreevy, R. L. (1993). *Solid State Ion.* **66**, 247–258.

Nield, V. M., Keen, D. A. & McGreevy, R. L. (1995). *Acta Cryst.* A**51**, 763–771.

Proffen, Th. & Neder, R. B. (1997). *J. Appl. Cryst.* In the press.

Proffen, Th., Neder, R. B. & Frey, F. (1996). *Acta Cryst.* B**52**, 59–65.

Proffen, Th., Neder, R. B., Frey, F. & Assmus, W. (1993). *Acta Cryst.* B**49**, 599–604.

Welberry, T. R. (1985). *Rep. Prog. Phys.* **48**, 1543–1593.

Welberry, T. R. & Butler, B. D. (1994). *J. Appl. Cryst.* **27**, 205–231.

Welberry, T. R. & Butler, B. D. (1995). *Chem. Rev.* **95**, 2369–2403.

Welberry, T. R., Butler, B. D., Thompson, J. G. & Withers, R. L. (1993). *J. Solid State Chem.* **106**, 461–475.

Welberry, T. R., Withers, R. L. & Mayo, S. C. (1995). *J. Solid State Chem.* **115**, 43–54.

Welberry, T. R., Withers, R. L., Thompson, J. G. & Butler, B. D. (1992). *J. Solid State Chem.* **100**, 71–89.